CrossMark

Effect of drying temperature on the structural and optical characteristics of Cu_2SnS_3 thin films synthesized by simple spin coating technique

S. Rabaoui[1] · H. Dahman[1] · S. Dekhil[1] · K. Omri[1] ·
A. Alyamani[2] · L. El Mir[1,3]

Abstract Thin films of Cu_2SnS_3 (CTS) were successfully prepared, by sol–gel spin coating technique on glass substrates. In this work, the effect of drying temperature on structural, morphological and optical characteristics is investigated. The X-ray diffraction patterns of the samples proved the polycrystalline nature and the formation of pure tetragonal Cu_2SnS_3 structure with (112) preferential orientation. The AFM and SEM images revealed that the CTS films have continuous and dense morphology. The average crystallite sizes calculated using the Debye–Scherrer formula increased from 3 to 6 nm and the direct optical band gap increased from 1.10 to 1.34 eV with increasing drying temperature from 150 to 300 °C. We found that by increasing the drying temperature, the sheet resistance decreased from 500 to 320 Ω. This makes the material as a good candidate for low cost and friendly environment thin film solar cells.

1 Introduction

Polycrystalline materials with semiconductor properties have special importance in the fabrication of low-cost solar cells, despite their lower conversion efficiency, when compared with the mono-crystalline Si solar cells [1–4]. Cu_2SnS_3 is one of the most promising ternary chalcopyrite materials, used as solar cell absorber [5, 6]. It has excellent physical and chemical properties such as an absorption coefficient of almost 10^4 cm^{-1} in the visible spectral range [7], tolerance to defects [8], chemical stability, a direct band gap of 1.3 eV (which is the optimum value for the photovoltaic conversion of solar energy [9]), and has possibility to be developed as n- or p-type semiconductor [10]. This material was successfully used in thin film solar cells with conversion efficiencies up to 11.4 % [11]. Many studies focused on developing correlations between the Cu_2SnS_3 materials deposition methods and the resulted structure, morphology and electrical conduction. However, for solar cell applications, it is challenging to obtain Cu_2SnS_3 in its pure kestrite phase [12]. A number of secondary and/or ternary phases like Cu_2S, SnS and Cu_3SnS_4 have been formed during the synthesis of Cu_2SnS_3. Moreover, the band gap grading, defects and uncontrolled stoichiometry along with secondary or ternary impurity phases can alter the optoelectronic properties of Cu_2SnS_3 [13]. A variety of techniques are reported to obtain Cu_2SnS_3 thin films, such as reactive radio frequency magnetron sputtering [12], co-evaporation [13], solvothermale [14], ion layer gas reaction [15], wet chemical process [16] and spray pyrolysis [17–19]. However, only a few papers report on sprayed Cu_2SnS_3 materials [20]. Compared with other techniques, the Spin coating method has many advantages such as low cost, simple synthesis equipment, easy fabrication of large-area, easier adjustment of composition. Especially, are suitable for the fabrication of thin films [16, 21]. How to prepare high-quality Cu_2SnS_3 thin films synthesized by simple spin coating technique has become a researches subject for a comparison between the structural and optical properties of nanocrystalline Cu_2SnS_3 thin films such as crystallite size and band gap energy.

✉ S. Rabaoui
  seif.rebaoui@yahoo.fr

1   Laboratory of Physics of Materials and Nanomaterials Applied at Environment (LaPhyMNE), Faculty of Sciences, Gabès University, 6072 Gabès, Tunisia

2   National Nanotechnology Research Centre, KACST, Riyadh, Saudi Arabia

3   Department of Physics, College of Sciences, Al Imam Mohammad Ibn Saud Islamic University (IMSIU), Riyadh 11623, Saudi Arabia

Hence this paper deals with pure tetragonal structure Cu_2SnS_3 films were grown by simple one-step spin coating technique. Structure and morphology of the obtained films are discussed on the basis of X-ray diffraction data, AFM and SEM respectively. The above properties have been reviewed with respect to the results of the sheet resistance. Optical characteristics are also reported.

2 Experimental procedure

2.1 Preparation of Cu_2SnS_3 Thin films

Thin CTS films were grown using spin coating route on glass substrates. The substrates was first cleaned by successive ultrasonic bath during 15 min, of acetone, deionised water and ethanol respectively and dried with jet dried-air. All the reagents and solvents were used without further purification. Copper acetate monohydrate $C_4H_6CuO_4 \cdot H_2O$ (1 mmol), tin chloride dehydrate $SnCl_2 \cdot 2H_2O$ (0.5 mmol) and thiourea H_2NCSNH_2 (1.5 mmol), were used as precursors for copper, tin and sulphur respectively. Further experimental details were given in our previous work [21]. The precursors were dissolved into 20 ml methanol and the mixture was then stirred at 60 °C during 2 h to yield a clear and homogenous solution. The resultant solution was spin-coated using the spin coater Model P6700. The films were dried in air on hot plate at constant time of 10 min for several drying temperatures 150 °C (S_1), 200 °C (S_2), 250 °C (S_3) and 300 °C (S_4). To obtain the final film, the spin coating and drying steps were repeated five times.

2.2 Characterization

The phase purity and crystal structure present in the samples materials was identified by using a Bruker D5005 diffractometer with CuKα radiation ($\lambda = 1.5418$ Å, 40 kV, 40 mA). The θ–2θ scans were recorded using a step size of 0.02° over the 2θ range between 20° and 60°. The morphology of the products was investigated out using Veeco DI CP-II Atomic Force Microscope and Field Emission Scanning Electron Microscope (FEI SEM, NNL 200, Japan). Room-temperature optical spectra in the wavelength range from 300 to 1500 nm were collected using a Schimadzu 3101 PC spectrophotometer. Four probe Lucas Labs-Pro4 was used to measure the sheet electrical resistance of the films. DekTak profilometer was used to measure film thickness and found to be 450–700 nm.

3 Results and discussion

3.1 Structural properties

Figure 1 shows the X-ray diffraction patterns of the synthesized thin films (CTS) for various drying temperature. For all recorded patterns, three pronounced diffraction peaks were observed at 2θ = 28.55°, 47.43° and 56.35° which can be attributed respectively to (112), (204) and (312) planes of Cu_2SnS_3 tetragonal structure according to JCPDS File n° 89–4714. Nevertheless, no characteristic peaks related to impurities were observed such as CuS, Cu_2S, SnS or Cu_3SnS_4, confirming that the obtained product is well crystallized and rather pure Cu_2SnS_3. The observed peaks indicate the polycrystalline nature of the materials. The presence of strong principal diffraction line corresponding to (112) plane indicates that the obtained films may have a preferential orientation. The average grain size was calculated using Scherrer's formula [22]:

$$G = \frac{0.9\lambda}{B \cos \theta_B} \tag{1}$$

where λ is the X-ray wavelength (1.5418 Å), θ_B is the maximum of the Bragg diffraction peak and B is the line-width at half maximum (in radians). In addition, the average crystallite sizes (G) of our samples at different temperature estimated using Scherrer and the lattice parameter (a) values are summarized in Table 1. The lattice parameters values are in good agreement with those reported by Fernandes et al. [23]. However they obtained grain sizes are comparable to those reported by Tiwari [24] and lower than those reported by Kahraman [25] and Yaşar [26] on samples synthesized by spin coating route.
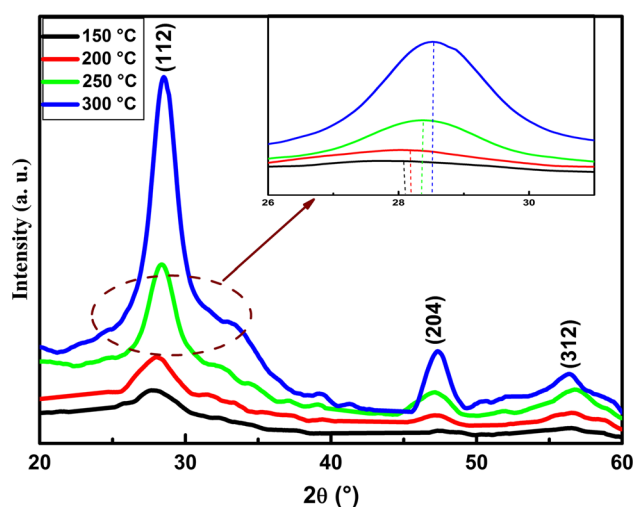

Fig. 1 XRD patterns of Cu_2SnS_3 thin films with different drying temperatures

Table 1 Variation of the grain size and lattice constant of the films Cu_2SnS_3 at different drying temperatures

Drying temperatures (°C)	Grain size (nm)	Lattice parameter (Å)	
		a = b	c
150	3	5.412	10.821
200	4	5.386	10.775
250	5	5.352	10.713
300	6	5.310	10.657

The evolution of the lattice parameters a calculated from the XRD for different drying temperature were studied. We observed a decrease in the lattice constant value with increasing drying temperature. This decrease of lattice constant is corroborated by the shift of the peaks position (inset in Fig. 1), Varieties of material structures have been reported in literature: cubic [27–30], tetragonal [31, 32], monoclinic [33] and triclinic [34, 35]. Nevertheless, one can note that our synthesis protocol seems to be the simplest one to obtain pure CTS thin films. Indeed, Kharaman et al. [25] Yaşar et al. [26] used many steps including sulfurization one at 550 °C, while Huan et al. [36] baked the synthesized films, at 80 °C for 5 min, then at 425 °C for 2 min and finally at 600 °C in sulfur atmosphere for 20 min.

3.2 Morphological properties

The surface morphology variation of the films deposited on glass substrates by 2D and 3D AFM are shown in Fig. 2. It is evident that the surfaces were rough compact without any visible cracks or holes. There are many nucleation centers on the substrate and small crystallites are produced. The root mean square (RMS) roughness for the Cu_2SnS_3 thin films, calculated by using the AFM equipment's software, are found to be 2.42, 4.26, 9.72 and 42.22 nm (Fig. 3) for an drying temperature of 150, 200, 250 and 300 °C respectively. This is due to the fact that with the increasing of drying temperature, the grain size increases and surface morphology becomes rougher. These characteristics are suitable to avoid shunting problems in solar cells. Furthermore, large grain size is preferred in the aim to reduce recombination at grain boundaries and involve carrier transport within the grain [37].

However SEM micrographs (Fig. 4) of samples surfaces were covered by homogeneous spherical shape microcrystallites. The microcrystallites diameters are ranging between 200 and 600 nm depending on drying temperature. Similar microcrystallites sizes (200–500 nm) were observed on surface samples grown using spray pyrolysis [38]. The observation was related to the possible vaporization of small drops during film growth. Droplets with dimensions ranging from hundreds of nanometers up to one micron have been observed on surfaces films synthesized by pulsed laser deposition route [39]. The observed grain size is higher than crystallite size calculated from XRD results using Scherrer equation. The difference between crystallite size and grain size was explained that grains may be formed by several crystallites. This phenomenon was also observed by other researchers, Elarbi et al. [40] in thermal evaporated $Sn_3Sb_2S_6$ thin films and Ares et al. [41] in polycrystalline pyrite films. In our case, the drying temperature seems to affect the surface quality of the deposited film and may be the cause of the presence of such forms. At increasing dying time more particles on the surface may agglomerate to form bigger grains. Other parameters such as drying time, solution viscosity and spinning speed may affect the surface film morphology.

3.3 Optical properties

Absorption spectroscopy is powerful technique to explore the optical properties of thin films. The measurements of transmittance and reflectance of the synthesized films in the wavelength range 300–1500 nm were shown in (Figs. 5, 6). One can notate that the sample transmittance decreases below 1400 nm while the reflectance decreases around 1200 nm. The absorption spectra of CTS films in the UV–visible-infrared range are shown in Fig. 7. Abroad optical absorption in the visible region and a tail extending to longer wavelengths can be observed from the measurement. The variation of the absorption coefficient versus the incident photon energy is shown in Fig. 8. It exhibits a large absorption on the order of $\alpha > 5 10^4$ cm^{-1} for S_2 and $\alpha > 6 10^4$ cm^{-1} for S_4 near the fundamental absorption edge.

The optical energy band gap 'E_g' is determined using the following relation, which is valid for direct band gap semiconductors [42].

$$(\alpha h\nu)^2 = A(h\nu - E_g) \tag{2}$$

where A is a constant, hν the photon energy and E_g is the energy band gap. From Eq. (2), a Tauc plot can be drawn of $(\alpha h\nu)^2$ versus hν. The point of the extrapolation of the linear part that meets the abscissa will give the value of the band gap energy (E_g) of the material (Fig. 9). The variation of E_g versus temperature and outlines a globally increasing in gap energy by increasing temperature. The obtained values 1.10 to 1.34 eV (Table 2), are suitable for photovoltaic solar conversion.

Furthermore, with increasing annealing temperature, the decrease of E_g should be related to the increase of grain

Fig. 2 AFM image
($5 \times 5 \ \mu m^2$) of Cu_2SnS_3 thin
films prepared with drying
temperatures
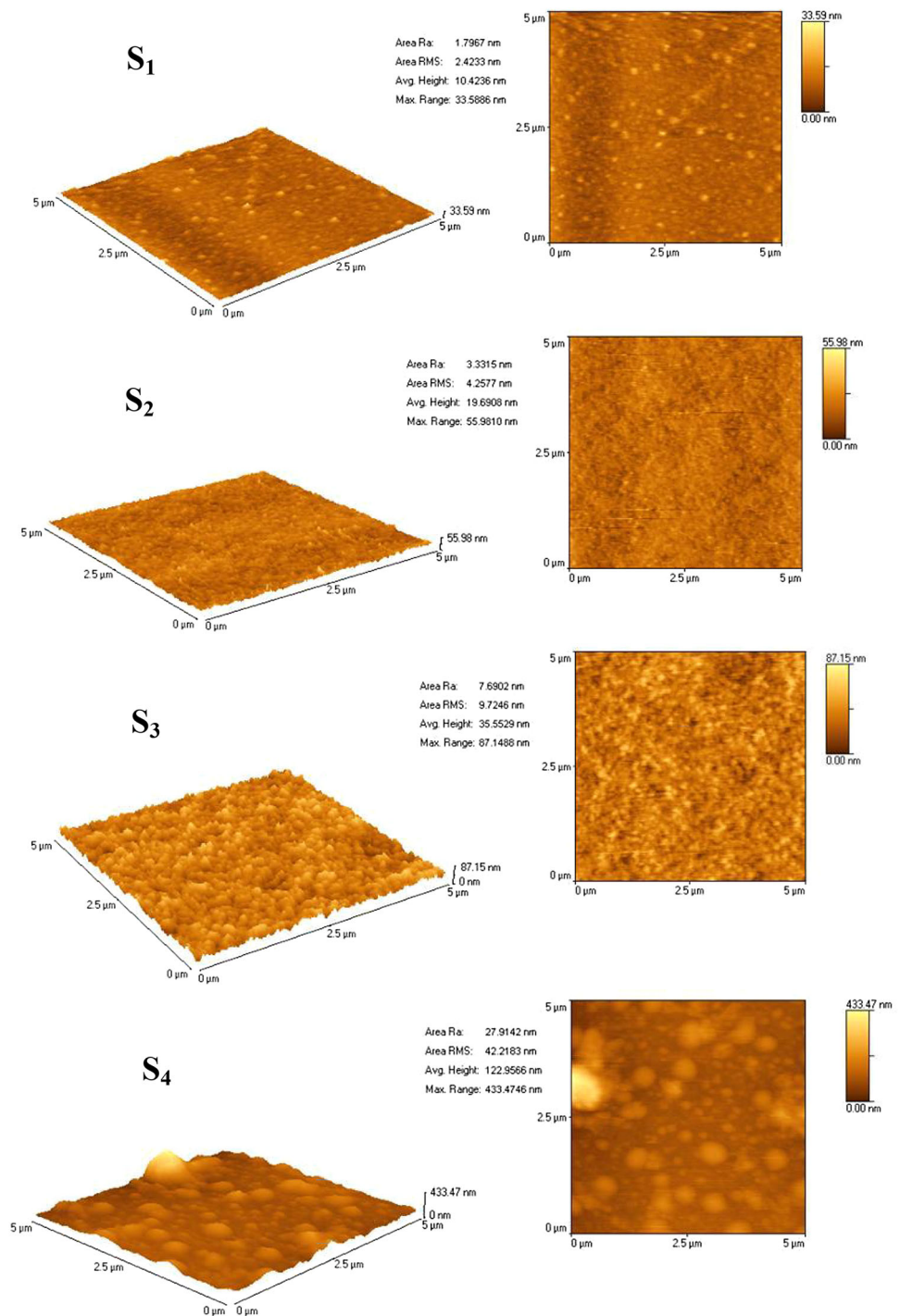
size and decrease of carrier concentration, and its decrease is also related to the decrease in the tensile stress. On the other hand, annealing process improve crystallinity and increase average grain size that result in decreasing defects, therefore band gap energy decreased. Decrease in band gap energy can be correlated with the XRD results.

The drying temperature is rather important. It may be an easy way to adjust the material's optical band gap by controlling the drying temperature. The near optimum band gap coupled with high absorption coefficient make CTS a potential absorber material for thin film solar cells [43, 44] and in good agreement with reported values obtained by
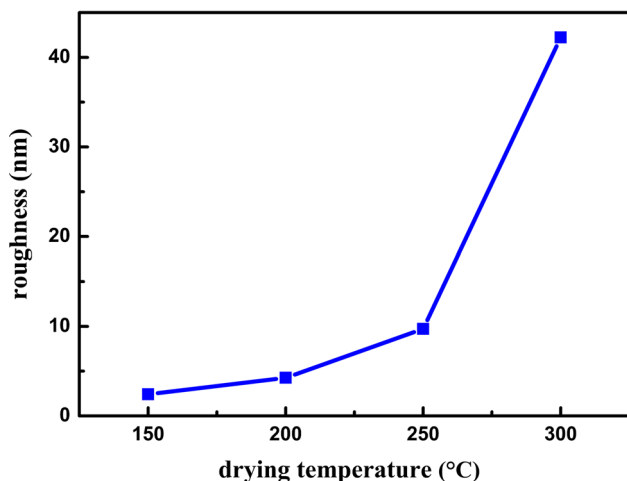
Fig. 3 Variation of the roughness (RMS) of Cu_2SnS_3 thin films as a function of the drying temperatures

Fig. 5 Transmittance spectra of Cu_2SnS_3 films deposited at various drying temperatures

spray pyrolysis 0.93–1.65 eV depending on grown temperature [45]. However, samples grown by RF magnetron sputtering at temperatures of 350–425 °C in hydrogen sulfide and nitrogen atmosphere, showed band gap in the range 1.77–2.19 eV [46].

3.4 Sheet resistance measurement

The film sheet resistance $R_\square$ variation versus drying temperature is shown in Table 2. A clearly increasing in $R_\square$ can be observed. The sheet resistance decreases from 500 to 320 Ω when drying temperature increases from 150 to 300 °C. The increase of the sheet resistance can be explained by the effect of drying temperature on the conductivity.
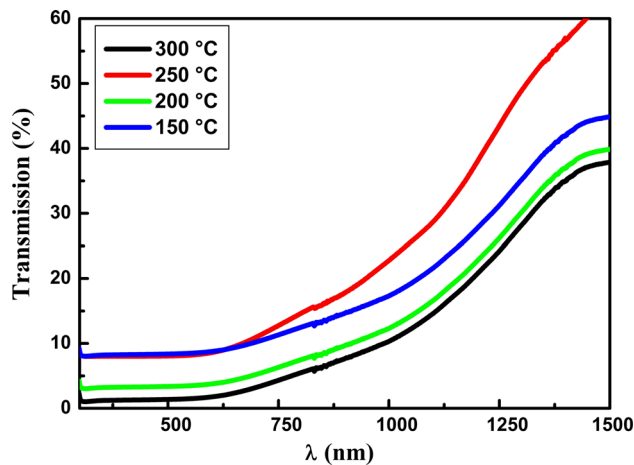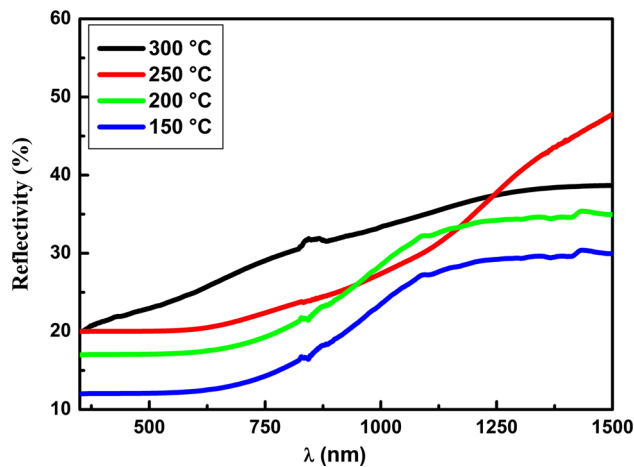

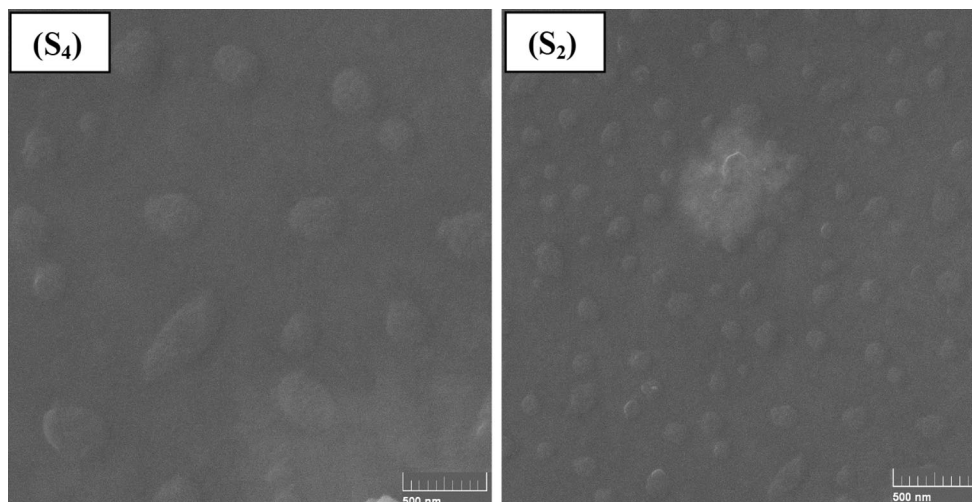Fig. 6 Reflectance spectra of Cu_2SnS_3 films deposited at various drying temperatures

Fig. 4 Typical SEM micrograph of Cu_2SnS_3 thin films prepared with drying temperatures: (S₂) 200 °C and (S₄) 300 °C
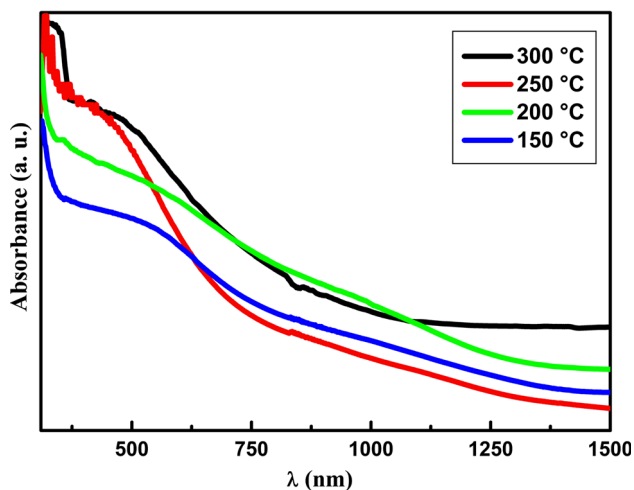
Fig. 7 Absorbance spectra of the deposited film of Cu_2SnS_3 with different drying temperatures

Fig. 9 Plots of $(\alpha h\nu)^2$ versus photon energy $h\nu$ of Cu_2SnS_3 thin films with various drying temperatures

4 Conclusion

Cu_2SnS_3 films were deposited on glass substrates by simple one-step spin coating technique. The effect of the drying temperature on the structural, optical and electrical properties of Cu_2SnS_3 films was investigated. All of the obtained films were polycrystalline with a tetragonal structure with (112) preferential orientation. SEM and AFM analysis revealed good surface morphology without any cracks or holes. The room temperature sheet resistance decreases significantly from 500 to 320 Ω with increasing drying temperature from 150 to 300 °C.

The optical band gap of these films is calculated. The deposited films exhibited high optical absorption coefficient in the visible range and a broad absorption in a wide
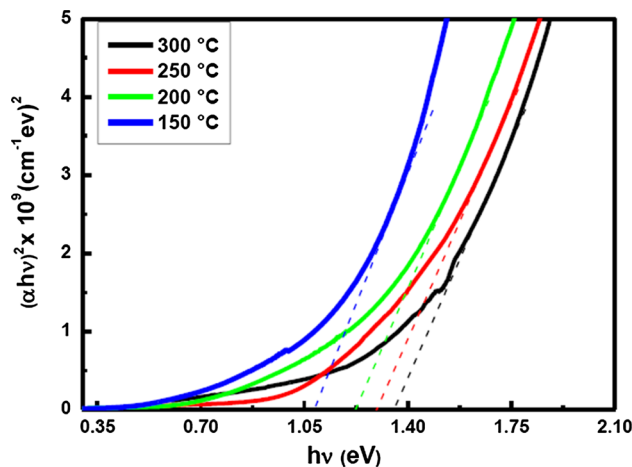
Table 2 Variation of the optical energy gap (E_g) and the sheet resistance $R_\square$ of the films Cu_2SnS_3 at different drying temperatures

Drying temperatures (°C)	150	200	250	300
E_g (eV)	1.10	1.22	1.30	1.34
$R_\square$ (Ω)	500	430	350	320

wavelength range from UV to visible light. We found that by increasing the drying temperature, the direct optical band gap increased from 1.10 to 1.34 eV which is optimum for photovoltaic solar conversion. Therefore, it is clear that Cu_2SnS_3 thin films deposited by spin coating technique can be very promising and are subsequently of great potential in the field of solar cells.
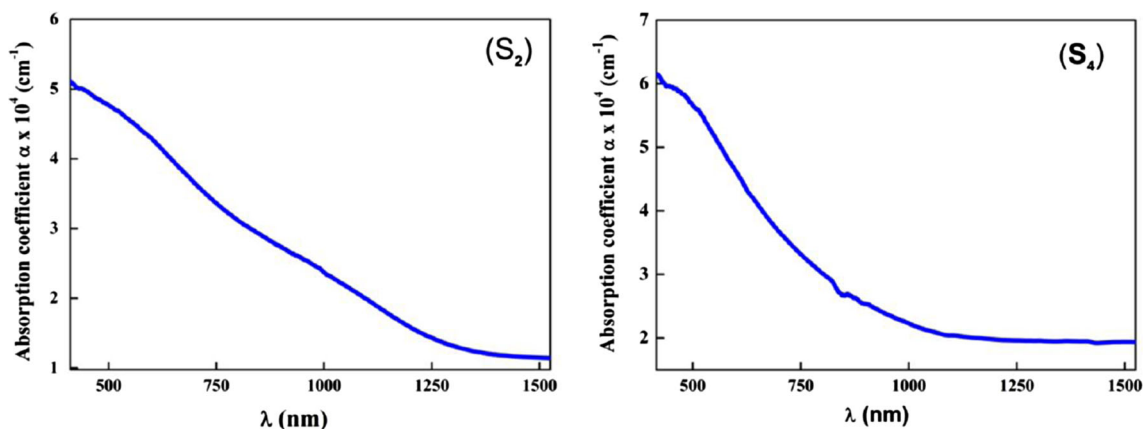

Fig. 8 Absorption coefficient versus photon energy $h\nu$ for the deposited samples of Cu_2SnS_3 with different drying temperatures: (S_2) 200 °C and (S_4) 300 °C

References

1. N. Aihara, H. Araki, A. Takeuchi, K. Jimbo, H. Katagiri, Phys. Status Solidi C **10**, 1086–1092 (2013)
2. T.P. Dhakal, C.Y. Peng, R.R. Tobias, R. Dasharathy, C.R. Westgate, Sol. Energy **100**, 23–30 (2014)
3. P. Jackson, D. Hariskos, E. Lotter, S. Paetel, R. Wuerz, R. Menner et al., Prog. Photovolt. **19**, 894–897 (2011)
4. S.A. Vanalakar, G.L. Agawane, S.W. Shin, M.P. Suryawanshi, K.V. Gurav, K.S. Jeon et al., J. Alloys Compd. **619**, 109–121 (2015)
5. X. Chang, H. Wada, A. Sato, M. Mieno, J. Solid State Chem. **139**, 144–148 (1998)
6. L. Kosyachenkoa, T. Toyama, Sol. Energy Mater. Sol. Cells **120**, 512–520 (2014)
7. D.B. Mitzi, O. Gunawan, T.K. Todorov, K. Wang, S. Guha, Sol. Energy Mater. Sol. Cells **95**, 1421–1436 (2011)
8. S. Abermann, Sol. Energy **94**, 37–70 (2013)
9. S.A. Vanalakar, S.J. Yeo, P.S. Patil, J.Y. Kim, J.H. Kim, Z. Phys. Chem. **228**, 917–926 (2014)
10. G.L. Agawane, S.W. Shin, S.A. Vanalakar, A.V. Moholkar, J.H. Kim, Mater. Lett. **37**, 147–149 (2014)
11. C.Z. Wu, Z.P. Hu, C.L. Wang, H. Sheng, J.L. Yang, Y. Xie, Appl. Phys. Lett. **91**, 143104–143106 (2007)
12. J.C. Zhou, L. You, S.W. Li, Y.L. Yang, Mater. Lett. **81**, 248–250 (2012)
13. Z. Seboui, A. Gassoumi, N.K. Turki, Mater. Sci. Semicond. Process. **26**, 360–366 (2014)
14. S. Rabaoui, H. Dahman, N. Ben Mansour, L. El Mir, J. Mater. Sci. Mater. Electron. **26**, 1119–1124 (2015)
15. A. Tombak, Y.S. Ocak, M.F. Genişel, T. Kilicoglu, Mater. Sci. Semicond. Process. **28**, 98–102 (2014)
16. K. Tanaka, Y. Fukui, N. Moritake, H. Uchiki, Sol. Energy Mater. Sol. Cells **95**, 838–842 (2011)
17. K. Woo, Y. Kim, J. Moon, Energy Environ. Sci. **5**, 5340–5345 (2012)
18. Q. Guo, H.W. Hillhouse, R.J. Agrawal, Am. Chem. Soc. **131**, 11672–11673 (2009)
19. Y. Zhou, W. Zhou, Y. Du, M. Li, S. Wu, Mater. Lett. **65**, 1535–1537 (2011)
20. Y. Wang, H.J. Gong, J. Alloys Compd. **509**, 9627–9630 (2011)
21. H. Dahman, S. Rabaoui, A. Alyamani, L. El Mir, Vacuum **101**, 208–211 (2014)
22. H. Saeki, H. Tabata, T. Kawai, Solid State Commun. **120**, 439–443 (2001)
23. P.A. Fernandes, P.M.P. Salome, A.F. da Cunha, J. Phys. D Appl. Phys. **43**, 215403–215414 (2010)
24. D. Tiwari, T.K. Chaudhuri, T. Shripathi, U. Deshpande, R. Rawat, Sol. Energy Mater. Sol. Cells **113**, 165–170 (2013)
25. S. Kahraman, S. Çetinkaya, S. Yaşar, İ. Bilican, Philos. Mag. **94**, 3149–3161 (2014)
26. S. Yaşar, S. Kahraman, S. Çetinkaya, İ. Bilican, J. Alloys Compd. **618**, 217–221 (2015)
27. B. Rezig, H. Dahman, M. Kenzar, J. Renew. Energy **2**, 125–128 (1992)
28. H. Dahman, M. Khalifa, B. Rezig, M. Brunel, Thin Solid Films **280**, 56–60 (1996)
29. G. Moh, Chem. Erde **34**, 1–61 (1975)
30. P.A. Fernandes, P.M.P. Salome, A.F. da Cunha, Phys. Status Solidi **7**, 901–904 (2010)
31. H. Hahn, H. Schulze, Naturwiss **52**, 426 (1965)
32. N. Wang, N. Jahrb, Mineral **241**, 424–431 (1974)
33. M. Onoda, X.A. Chen, A. Sato, H. Wada, Mater. Res. Bull. **35**, 1563–1570 (2000)
34. X. Chen, X. Wang, C. An, J. Liu, Y. Qian, J. Cryst. Growth **256**, 368–376 (2003)
35. D. Avallaneda, M.T.S. Nair, P.K. Nair, J. Electrochem. Soc. **187**, 346–352 (2010)
36. J. Han, Y. Zhou, Y. Tian, Z. Huang, X. Wang, J. Zhong, Z. Xia, B. Yang, H. Song, J. Tang, Front. Optoelectron. **7**, 37–45 (2014)
37. Q.W. Tian, X.F. Xu, L.B. Han, M.H. Tang, R.J. Zou, Z.G. Chen, M.H. Yu, J.M. Yang, J.Q. Hu, Cryst. Eng. Commun. **14**, 3847–3850 (2012)
38. M. Bouaziz, K. Boubaker, M. Amlouk, S. Belgacem, J. Phase Equilib. Diffus. **31**, 498–503 (2010)
39. R.B. Ettlinger, A. Cazzaniga, S. Canulescu, N. Pryds, J. Schou, Appl. Surf. Sci. **336**, 385–390 (2015)
40. A. Larbi, H. Dahman, M. Kanzari, Vacuum **110**, 34–39 (2014)
41. J.R. Ares, A. Pascual, I.J. Ferrer, C. Sánchez, Thin Solid Films **480**, 477–481 (2005)
42. C.H.L. Weijtens, P.A.C. Vanloon, Thin Solid Films **196**, 1–10 (1991)
43. D. Tiwari, T.K. Chaudhuri, T. Shripathi, U. Deshpande, R. Rawat, Sol. Energy Mater. Sol. Cells **113**, 165–170 (2013)
44. K. Tanaka, Y. Fukui, N. Moritake, H. Uchiki, Sol. Energy Mater. Sol. Cells **95**, 838–842 (2011)
45. U. Chalapathi, Y. Jayasree, S. Uthanna, V. Sundara Raja, Phys. Status Solidi A **210**, 2384–2390 (2013)
46. P. Zhao, S. Cheng, Adv. Mater. Sci. Eng. **2013**, 726080–726084 (2013)